



# An accurate mathematical model for ball end mills with chisel edge

Hongyang Wang<sup>1</sup> · Xianli Liu<sup>1</sup> · Caixu Yue<sup>1</sup> · Zhipeng Jiang<sup>1</sup> · Gaojun Zheng<sup>1</sup> · Kaiwang Zhao<sup>1</sup>

Received: 9 July 2023 / Accepted: 26 December 2023 / Published online: 4 March 2024  
© The Author(s), under exclusive licence to Springer-Verlag London Ltd., part of Springer Nature 2024

## Abstract

Ball end mills have complex geometry. The precision CNC grinding of the cutting edge on the spherical surface is a big challenge for the tool manufacturers. Regarding the design cutting edge, we propose a cutting-edge design model in which the cutting edge can be offset along the spherical surface. To improve the accuracy of this model, the twist drill chisel-edge was also introduced into this design model of cutting edge. Then, referring to the toolpath calculation method of complex surface machining, we established a method for grinding the rake face of the ball end mill using a 1A1 standard wheel. For the clearance of the ball end mill, we developed a method to grind the clearance of the ball end mill using an 11V9 standard wheel. Finally, the design model of cutting edge, grinding models of rake face, and clearance were verified by simulations and experiments, respectively. The results show the proposed cutting-edge model has a better profile tolerance. The intersection line between the rake face and clearance coincides with the design's cutting edge. These prove the effectiveness of methods.

**Keywords** Ball end mill · Mathematical model · CNC grinding · Chisel edge

## 1 Introduction

As we all know, ball end mill was widely used in the manufacturing industry, such as mold and die, aerospace, and electronics. The ball end mill includes two parts: the ball part and the cylindrical part. The cylindrical part is similar to the end mill. The algorithm for the design and manufacture of this part is well-developed [1–4]. Although the designing and manufacturing of the ball part have been paid attention to by scholars, there are still some issues. According to the type of cutting edge, the ball end mill contains planar edge ball end mill and helical edge ball end mill. The cutting edge of the plane edge ball end mill is formed by the intersection of the spherical surface and plane through the axis of the spherical surface. The helical edge is built in more complex ways. The cutting edge is the intersection of the helical surface and the spherical surface or the spherical curve with constant pitch and helix angle. Hien Nguyen et al. [5] derived a cutting-edge curve with an equal pitch on the spherical surface. This curve has a constant ratio of axial

motion speed to radial rotation speed. Chen et al. [6] established a cutting-edge curve with an equal helix angle, which is defined as the angle between the tangent of the edge and the tangent of the generatrix that generates the tool's rotating surface. Lin et al. [7] also built a cutting-edge curve with an equal helix angle, which is defined as the angle between the tangent of the edge and the axis of the spherical surface. Yi Lu et al. [8] established the cutting-edge curve by the intersection of the vertical line and the spherical surface. The cutting edge of the above model must be over the vertex of the spherical surface. However, the cutting edge of the ball end mill has an offset distance in practice. Therefore, a cutting-edge model with offset distance was proposed [8]. The profile tolerance of this cutting-edge is weak at the vertex of the ball.

The intersection of the clearance and rake face is the cutting edge. The grinding trajectory of the rake face and clearance is very important to the manufacturing model, which significantly affects the profile tolerance of the ball end mill. Adjustment of the axial speed, radial speed, and compensatory operation of the wheel is made to grind the ball end mill in a two-axis NC machine [9]. However, using this method to grind the ball end mill, we require compensation of grinding path based on the simulation result, and it is difficult to grind the designed cutting edge directly. Taking advantage of the developable surfaces, many scholars brought

✉ Xianli Liu  
xianli.liu@hrbust.edu.cn

<sup>1</sup> School of Mechanical and Power Engineering, Harbin University of Science and Technology, Harbin 150080, China

the developable surface into the design and manufacturing model of ball end mills. Taking the constant lead cutting edge as an example, Hein Nguyen et al. [5] established the developable rake face and the developable clearance. Then, he built the method of grinding the rake face with a 1A1 wheel and the method of grinding the clearance face with an 11V9 wheel. For other cutting edges, it is difficult to meet the requirements of the developable surface, so it limits the popularization and application of the method directly. Xiong et al. [10] ground the rake face of a tapered ball end mill along the frenet frame of the cutting edge. The width of the rake face is determined by the wheel chamfer and the grinding point. Relying on the constant curvature of the spherical wheel, Chen et al. [6] ground the rake face of the tapered ball end mill with this wheel and reduced the number of machine axis required from five to four. Large chamfer wheels and spherical wheels are non-standard grinding wheels, making them difficult to be popularized for practical applications. To strengthen the cutting edge, Ji Wei et al. [11] and Yi Lu et al. [12] developed a mathematical model of the chamfer of the cutting edge of the ball end mill respectively, which belongs to the developable surfaces. The above model has lower strength at the vertex part of the ball end mill, because the offset distance was not considered. If the offset distance is considered, the profile tolerance will be poor at the vertex of the ball end mill.

To solve these problems, a novel manufacturing model of the ball end mill is proposed in this paper. In Section 2, this paper introduces the chisel-edge of twist drill into the ball end mill (shown in Fig. 1), which allows the cutting-edge of ball end mill to have an offset distance and the ball end mill has a better profile tolerance at the same time. Then, the method of grinding the rake face and clearance using a standard wheel are determined in Section 3. Finally, the designed model is verified with grinding experiments and simulations in Section 4.

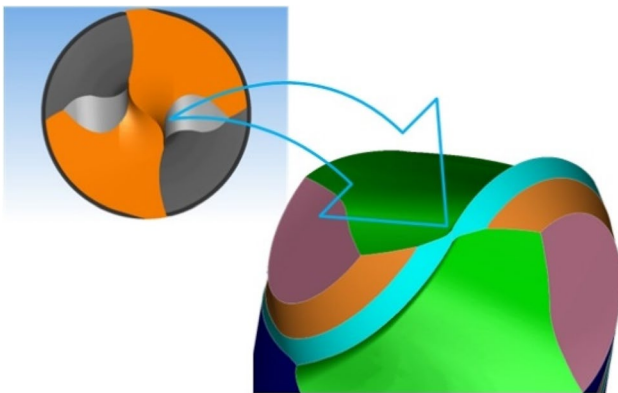


Fig. 1 The twist drill chisel-edge and ball end mill

## 2 The mathematical model for cutting edge and wheel

The profile tolerance of tool is related to the grinding machine. It is also influenced by the accuracy of the mathematical model. Therefore, an accurate mathematical model is essential. In this chapter, the models of the cutting edge are determined.

### 2.1 Cutting edge for rake face

As shown in Fig. 2, O-XYZ is the global coordinate system, and the Z-axis coincides with the axis of the tool. In this system, the edge is expressed as:

$$\begin{cases} x = R_t \cos \theta \\ y = R_t \sin \theta \\ z = z \end{cases} \quad (1)$$

where the angle  $\theta$  is the circumferential angle of the projection of the point in XOY plane.  $R_t$  is the radius of the tool, is a function of  $z$ . It is expressed as:

$$R_t = \sqrt{R^2 - z^2} \quad (2)$$

The helix angle of the cutting edge: the angle between the tangent of the edge and the tangent of the generatrix that generates the tool's rotating surface. The helix angle is 0 for  $z=R$ . The helix angle is  $\beta_0$  for  $z=0$ . The helix angle varies linearly with  $z$  (which can also be non-linear). It can be expressed as:

$$\beta(z) = \frac{R-z}{R} \beta_0 \quad (3)$$

As we all know, the helix angle is equal to the angle between the speed of the cutting edge and the speed along the generatrix.

$$\tan \beta(z) = \frac{\sqrt{R^2 - z^2} \frac{d\theta}{dt}}{\frac{ds}{dt}} = \frac{\sqrt{R^2 - z^2} d\theta}{ds} \quad (4)$$

where  $ds = \sqrt{d^2z + d^2\sqrt{R^2 - z^2}}$ .  $\theta$  is given by:

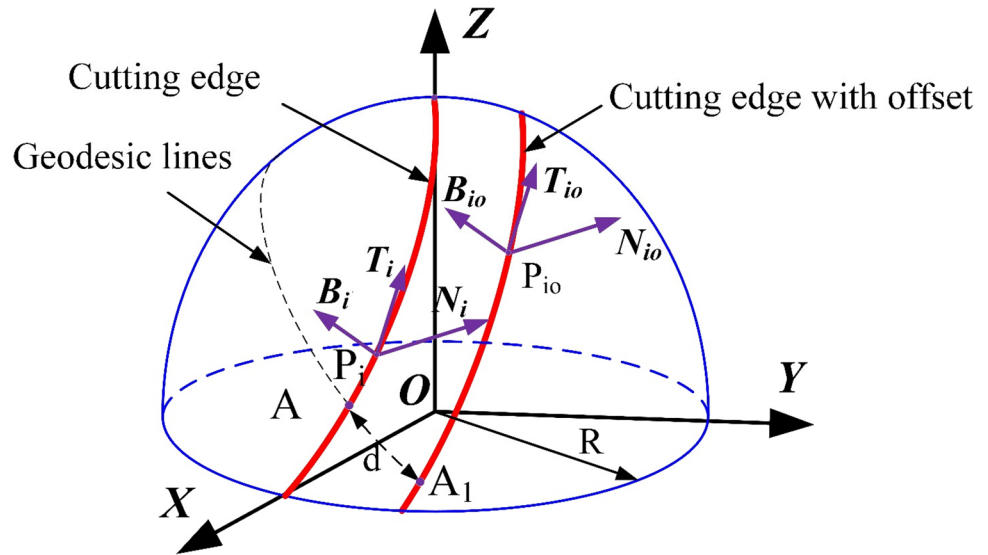
$$\theta = \int_0^z \tan(\beta(z)) \frac{R}{R^2 - z^2} dz \quad (5)$$

The space curve frame is essential for this paper. It can describe the relative position conveniently. Take any point  $P_i$  on the cutting edge, we establish a frame  $P_i-T_i-B_i-N_i$  at this point.  $P_i$  is given by

$$P = [x_p \ y_p \ z_p]^T \quad (6)$$

The  $T_i$  is the tangent vector of the cutting edge at  $P_i$  point. The  $N_i$  is the normal vector of the spherical surface at  $P_i$  point,

**Fig. 2** The cutting edge and the coordinate system



direction from inside the ball to outside the ball. We define the binormal vector  $B_i$  as the vector product of  $T_i$  and  $N_i$ .

To get the cutting-edge curve with an offset distance, the cutting edge curve moves the distance  $d$  along the geodesic curve of the spherical surface in this paper. It is known from differential geometry, the geodesic curve of the spherical surface is a circle whose radius is  $R$  and passes through the selected point. The cutting edge curve with offset can be expressed as

$$R_1(\theta) = R(\theta) - R \sin \theta_1 B - R(1 - \cos \theta_1)N \tag{7}$$

where  $\theta_1 = d/R$ . From Appendix A, curve  $R_1(\theta)$  has the same tangent vector as the original curve  $R(\theta)$ . Take any point  $P_{i0}$  on the cutting edge, we establish a frame  $P_{i0}-T_{i0}B_{i0}N_{i0}$  at this point.  $P_{i0}$  is given by

$$P_{i0} = [x_{p0} \ y_{p0} \ z_{p0}]^T \tag{8}$$

The  $T_{i0}$  is the tangent vector of the cutting edge  $R_1$  at  $P_{i0}$  point. The  $N_{i0}$  is the normal vector of the spherical surface at  $P_{i0}$  point, direction from inside the ball to outside the ball. We define the binormal vector  $B_{i0}$  as the vector product of  $T_{i0}$  and  $N_{i0}$ . According to the relationship between the global coordinate system and the frame  $P_{i0}-T_{i0}B_{i0}N_{i0}$ , we can get the rotational matrix  $M_1$  and the translational matrix  $R_1$ .

$$M_1 = \begin{bmatrix} 1 & 0 & 0 & x_{p0} \\ 0 & 1 & 0 & y_{p0} \\ 0 & 0 & 1 & z_{p0} \\ 0 & 0 & 0 & 1 \end{bmatrix} \text{ and } R_1 = \begin{bmatrix} T_{i0x} & B_{i0x} & N_{i0x} & 0 \\ T_{i0y} & B_{i0y} & N_{i0y} & 0 \\ T_{i0z} & B_{i0z} & N_{i0z} & 0 \\ 0 & 0 & 0 & 1 \end{bmatrix} \tag{9}$$

### 2.2 Cutting edge for clearance

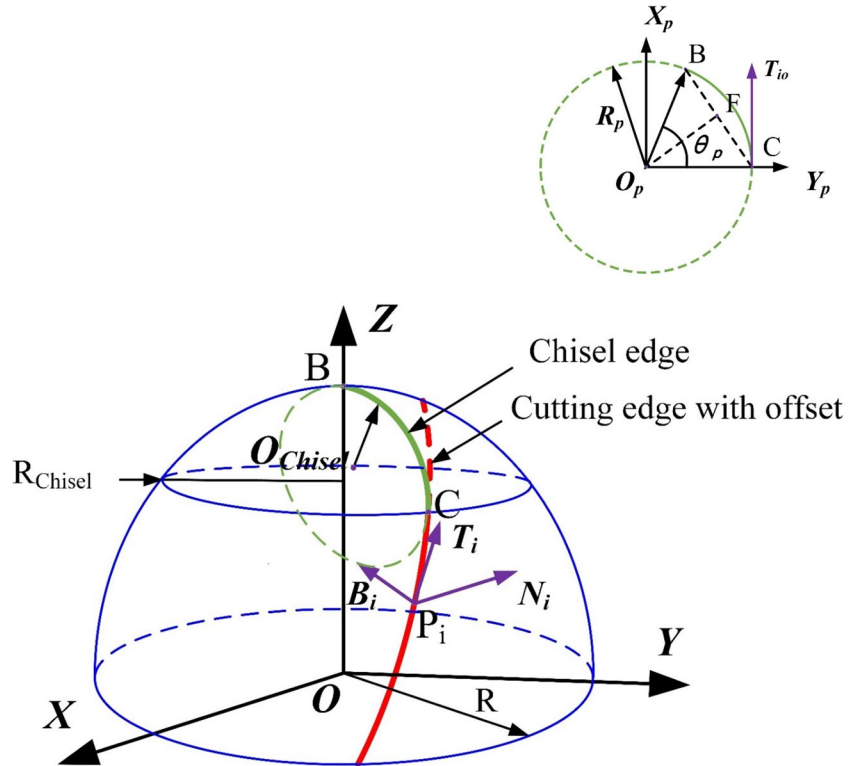
As the cutting edge moves along the spherical, the cutting edge does not pass the vertex of the spherical surface. The profile tolerance of the cutting edge at the vertex of the spherical surface is poor, this may lead to out-of-tolerance of this part. Therefore, the concept of twist drill chisel-edge is introduced into the model of the clearance in this paper. In other words, the cutting-edge curve is modified, as shown in Fig. 3.  $BC$  is a chisel-edge, where point  $C$  is the beginning of the chisel-edge and point  $B$  is the vertex of the spherical surface.  $BC$  is the intersection line between the spherical surface and plane, the plane passes  $T_{i0}$  at point  $C$  and  $\overline{BC}$ . The distance of point  $C$  from the axis of  $Z$  is  $R_{Chisel}$ . The property of the spherical surface,  $BC$  is a part of the circle.

We establish the coordinate system  $O_p-X_pY_pZ_p$  at point  $O_p$ ,  $X_p$  is parallel to  $T_{i0}$ ,  $Y_p$  is parallel to  $O_pC$ , the vector  $Z_p$  as the vector product of  $X_p$  and  $Y_p$ ,  $O_p-X_pY_pZ_p$  satisfies the right-hand rule. In this system,  $BC$  is expressed as

$$R_{BC} = \begin{bmatrix} x_{Chisel} \\ y_{Chisel} \\ z_{Chisel} \\ 1 \end{bmatrix} = \begin{bmatrix} X_{px} & Y_{px} & Z_{px} & O_{px} \\ X_{py} & Y_{py} & Z_{py} & O_{py} \\ X_{pz} & Y_{pz} & Z_{pz} & O_{pz} \\ 0 & 0 & 0 & 1 \end{bmatrix} \begin{bmatrix} R_p \sin \theta_c \\ R_p \cos \theta_c \\ 0 \\ 1 \end{bmatrix} \tag{10}$$

where the angle  $\theta_c$  is the circumferential angle of the projection of the point in the  $O_p-X_pY_pZ_p$  plane. Along the chisel-edge curve, we can also obtain the frame and matrix similar to the cutting edge.

**Fig. 3** The chisel-edge of ball end mill



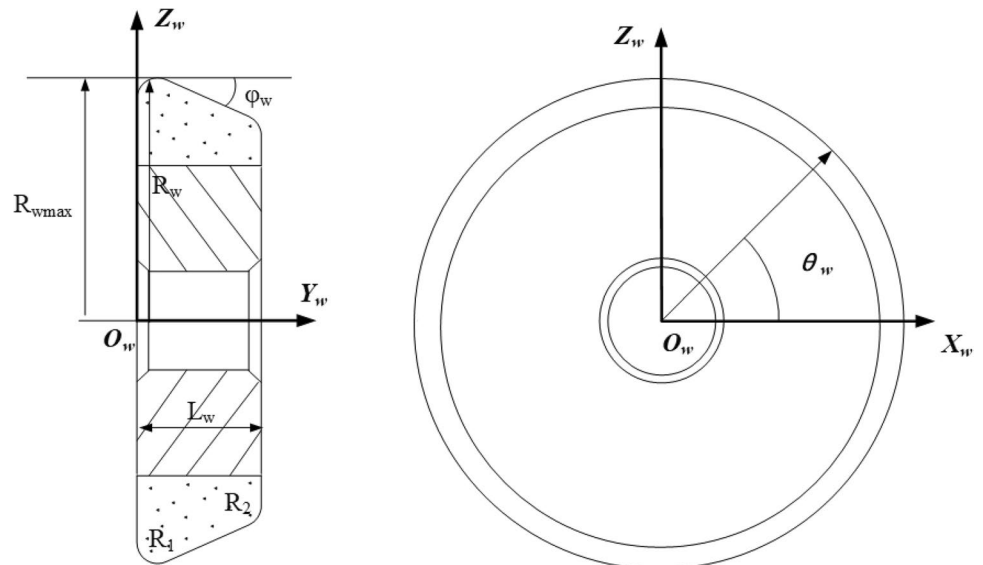
**2.3 The coordinate of wheel**

To represent the wheel’s revolving surface, a coordinate system is established. As shown in Fig. 4,  $O_w-X_wY_wZ_w$  is the coordinate system of wheel, and the Y-axis coincides with the axis of wheel. In this system, the surface of wheel is expressed as

$$\begin{cases} x_w = R_w \cos \theta_w \\ y_w = y \\ z_w = R_w \sin \theta_w \end{cases} \quad (11)$$

where the angle  $\theta_w$  is the circumferential angle of the projection of point in  $O_wX_wZ_w$  plane.  $R_w$  is the radius of wheel, is a function of  $y$ . It is expressed as

**Fig. 4** The coordinate of wheel



$$R_w = \begin{cases} R_{w\max} + R_1(\sin(\arccos \frac{R_1 - y}{R_1}) - 1) & 0 \leq y < R_1 \\ R_{w\max} + R_1(\sin(\arccos \frac{y - R_1}{R_1}) - 1) & R_1 \leq y < R_1(1 + \sin \varphi_w) \\ R_{w\max} + R_1(\cos \varphi_w - 1) - (y - R_1(\sin \varphi_w + 1))\tan \varphi_w & R_1(1 + \sin \varphi_w) \leq y < L_w - R_2(1 - \sin \varphi_w) \\ R_{w\max} + R_1(\cos \varphi_w - 1) - (L_w - R_2(1 - \sin \varphi_w)) - R_1(\sin \varphi_w + 1)\tan \varphi_w + R_2(\sin(\arccos \frac{y - (L_w - R_2)}{R_2}) - 1) & L_w - R_2(1 - \sin \varphi_w) \leq y \leq L_w \end{cases} \quad (12)$$

### 3 The mathematical model for machining ball end mill

This section describes the calculation of the wheel posture for the rake face and clearance of the ball end mill. When machining a surface on a 5-axis machine, the tool moves along the curve of the machining surface. The idea is applied to calculate the grinding trajectory of ball end mills in this paper. In other words, the wheel moves along the cutting edge. The rake face is ground with a 1A1 wheel (as shown in Fig. 5). The clearance is ground with an 11V9 wheel (as shown in Fig. 7).

### 3.1 The mathematical model for grinding rake face

The procedure of the method that calculates the position of wheel is as follows:

Step 1: The cutting edge is discretized into points. The number of points affects the simulation and grinding accuracy. Then, we can easily calculate the frame at each point. Any point  $P_i$  is selected as the current grinding point of the cutting edge.

Step 2: Select any point on the arc chamfer of wheel, we define this point as the grinding point  $G$ .  $G$  can be rep-

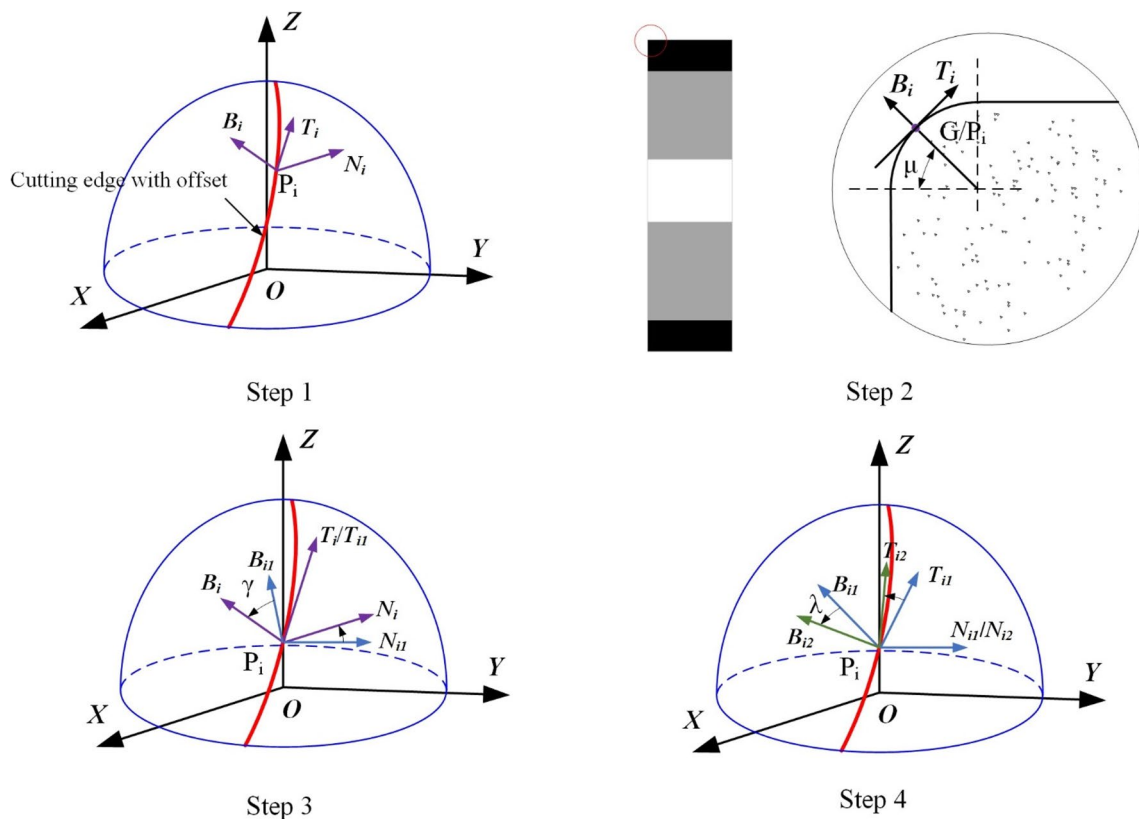
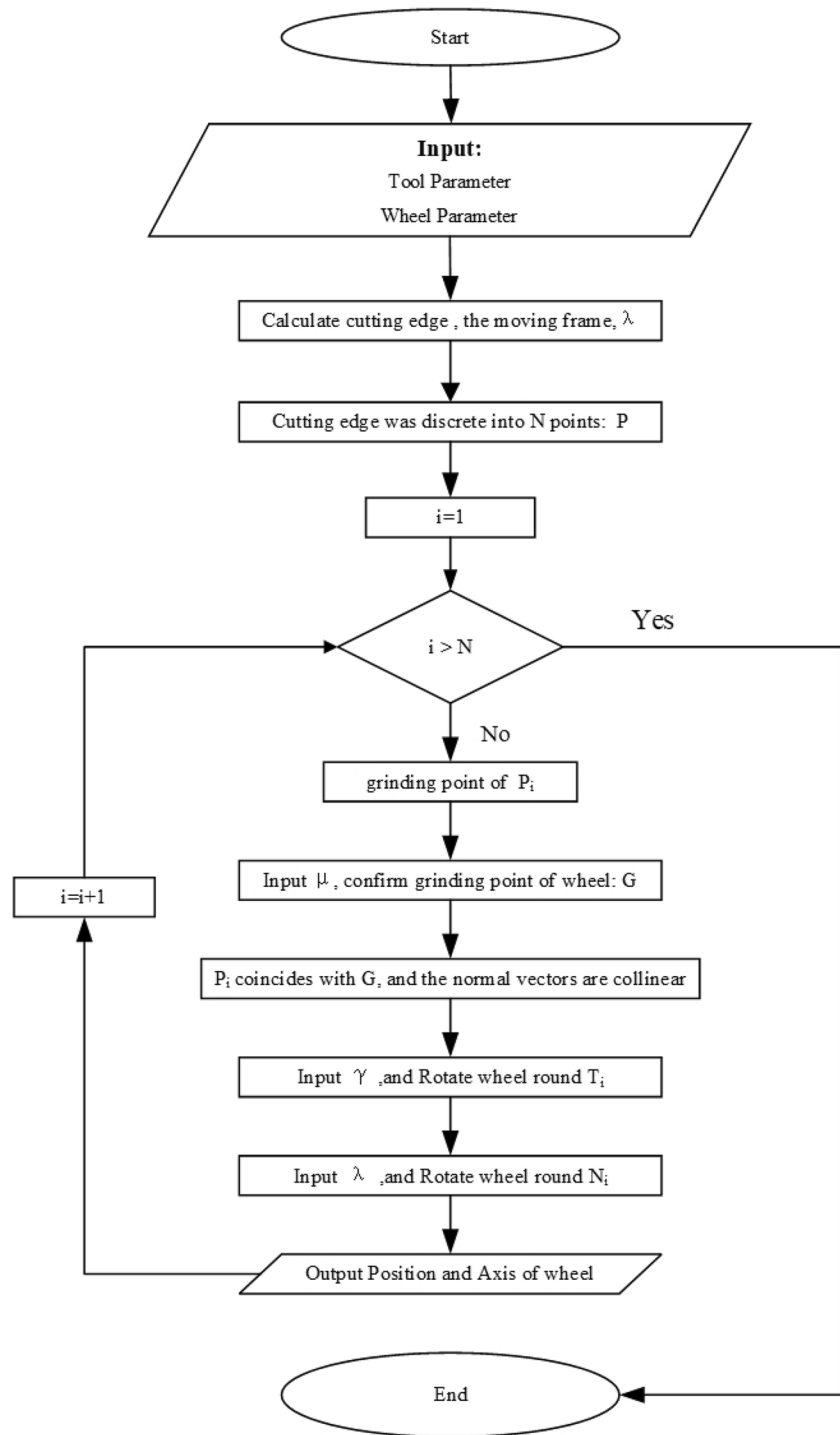


Fig. 5 The calculation of wheel position for rake face

**Fig. 6** Principle of calculating the grinding path for the rake face



resented in the coordinate system of wheel by equation  $[x_G \ y_G \ z_G]^T$  (Fig. 5). The angle  $\mu$  is the angle between the normal vector of the  $G$  and the axis of wheel, is a constant. The initial position of wheel is shown in Fig. 5. This position must satisfy the following requirements:

- The grinding point  $G$  must coincide with  $P_i$  that the origin of the frame.
- The normal vector of  $G$  and the binormal vector  $B_i$  are collinear.
- The axis of wheel must be in the plane that the plane contains  $B_i$ ,  $P_i$ , and  $T_i$ .



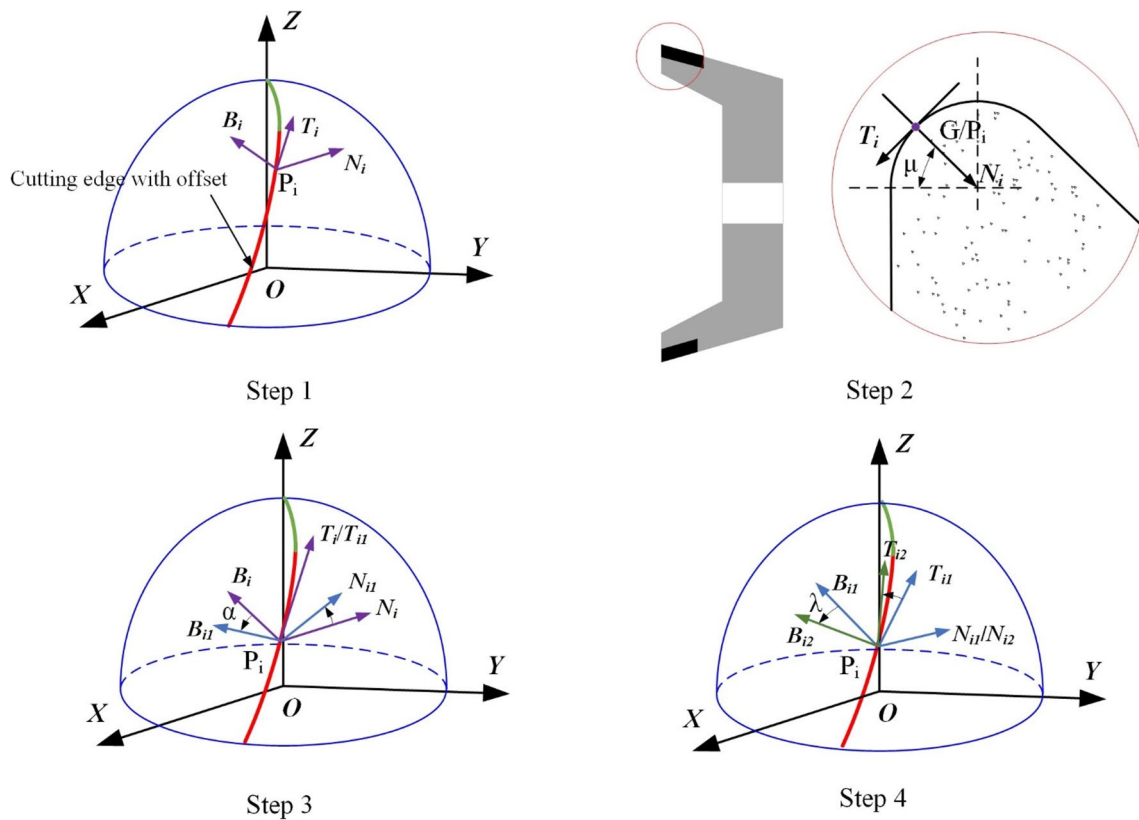


Fig. 7 The calculation of wheel position for clearance

The rotational matrix  $R_2$  and the translational matrix  $M_2$  describe translation and rotation from  $O_w-X_wY_wZ_w$  to  $P_i-T_iB_iN_i$  and are represented by:

$$M_2 = \begin{bmatrix} 1 & 0 & 0 & x_G \\ 0 & 1 & 0 & y_G \\ 0 & 0 & 1 & z_G \\ 0 & 0 & 0 & 1 \end{bmatrix} \text{ and } R_2 = \begin{bmatrix} 0 & \sin \mu & \cos \mu & 0 \\ 0 & -\cos \mu & \sin \mu & 0 \\ 1 & 0 & 0 & 0 \\ 0 & 0 & 0 & 1 \end{bmatrix} \quad (13)$$

Step 3: To get the rake angle on the rake face, we rotate the wheel and the frame around  $T_i$  by  $\gamma$  together.  $\gamma$  can be continuously varied during the grinding process.  $\gamma$  is equal to rake angle (for details, see Chapter 4). We obtain a new frame  $P_{i1}-T_{i1}B_{i1}N_{i1}$ . Like Step 2, we can get the rotational matrix  $R_3$ , which is given by:

$$R_3 = \begin{bmatrix} 1 & 0 & 0 & 0 \\ 0 & \cos \gamma & -\sin \gamma & 0 \\ 0 & \sin \gamma & \cos \gamma & 0 \\ 0 & 0 & 0 & 1 \end{bmatrix} \quad (14)$$

Step 4: The material removal is very high in the above wheel position. This affects the strength of the tool. At the same time, the wheel collides with the cylindrical part of the ball end mill. Therefore, the wheel and

the frame are rotated around  $N_i$  by  $\lambda$ . The calculation method of  $\lambda$  is shown in Appendix B. The new frame is defined as  $P_{i2}-T_{i2}B_{i2}N_{i2}$ . Similarly, the rotational matrix  $R_4$  is represented

$$R_4 = \begin{bmatrix} \cos \lambda & -\sin \lambda & 0 & 0 \\ \sin \lambda & \cos \lambda & 0 & 0 \\ 0 & 0 & 1 & 0 \\ 0 & 0 & 0 & 1 \end{bmatrix} \quad (15)$$

The center position of the wheel can be expressed in the global coordinate system  $O-XYZ$  as

$$\begin{bmatrix} X_{Center} \\ Y_{Center} \\ Z_{Center} \\ 0 \end{bmatrix} = M_1 \cdot R_1 \cdot R_3 \cdot R_4 \cdot R_2 \cdot \left( M_2 \cdot \begin{bmatrix} x_w \\ y_w \\ z_w \\ 1 \end{bmatrix} \right) \quad (16)$$

The axis of the wheel can be expressed in the global coordinate system  $O-XYZ$  as

$$\begin{bmatrix} X_{Axis} \\ Y_{Axis} \\ Z_{Axis} \\ 0 \end{bmatrix} = M_1 \cdot R_1 \cdot R_3 \cdot R_4 \cdot R_2 \cdot \left( M_2 \cdot \begin{bmatrix} 0 \\ 1 \\ 0 \\ 0 \end{bmatrix} \right) \quad (17)$$

**Fig. 8** Principle of calculating the grinding path for the clearance

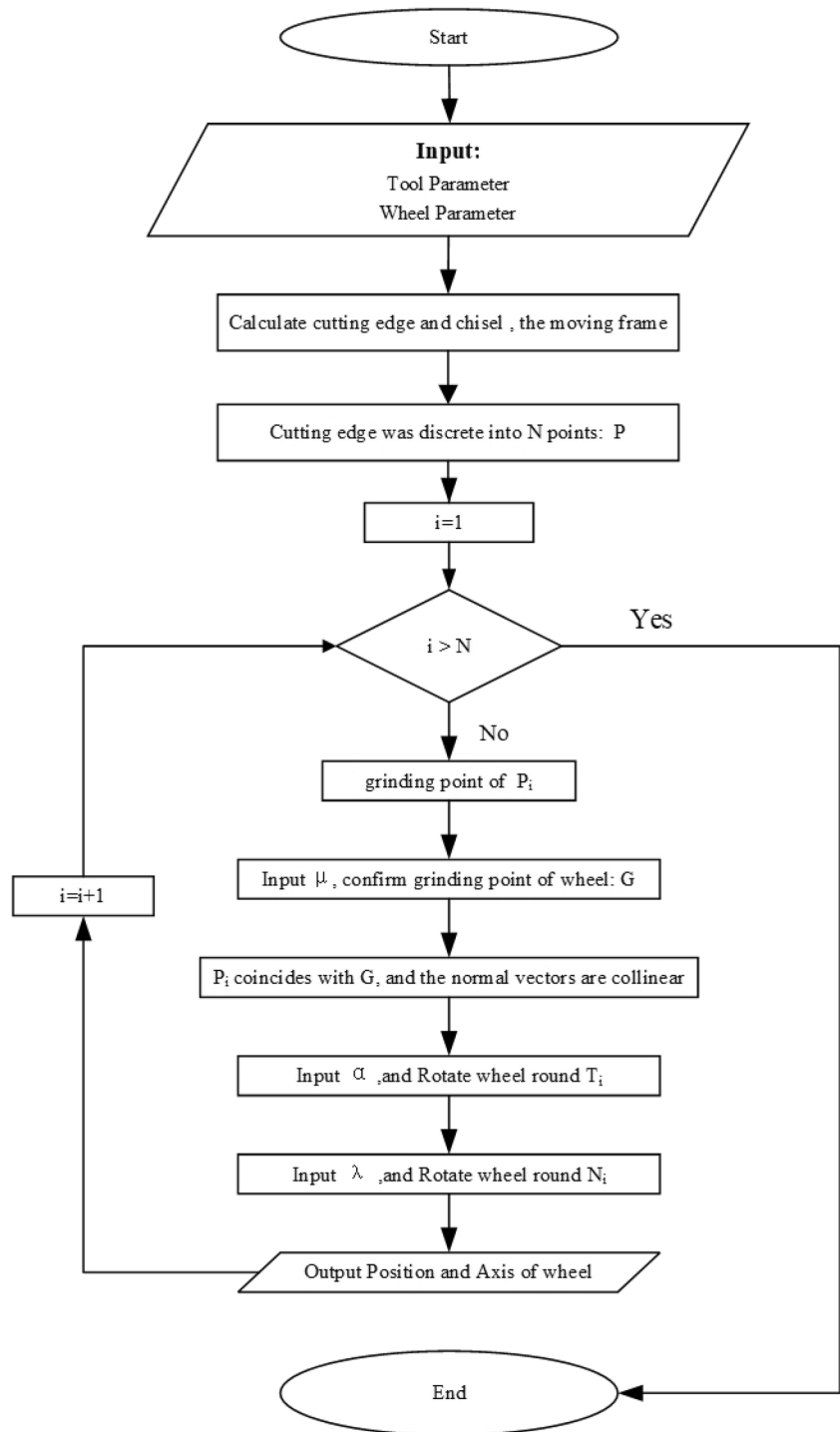


Figure 6 shows the process of calculating the trajectory of the rake face for the ball end mill.

### 3.2 The mathematical model for grinding clearance

As can be known in Section 2, the cutting edge consists of two parts: the chisel-edge and the main cutting edge for clearance.

The chisel-edge is formed by the intersection of the clearance. So, the first point of the chisel-edge of the opposite cutting edge is the grinding start point. Only in this way, the clearance and chisel-edge can be ground together. The procedure of the method that calculates the position of wheel is as follows:

Step 1: Same as step 1 of the rake face. The cutting edge is discretized into points. Then, we can calculate



**Table 1** The parameters of the ball end mill

	Diameter (mm)	Helix ( $Z=0$ )	Helix ( $Z=R$ )	Rake ( $^\circ$ )	Teeth	Radius of chisel (mm)	Side distance (mm)
Case 1	12	30	0	5	2	0.5	0.3
Case2	12	30	0	5	2	1	0.3
Case3	12	30	0	5	2	/	0.3
	Tip clearance Relief ( $^\circ$ )	Width (mm)	Dis <sub>A</sub> (mm)	Dis <sub>B</sub> (mm)	Angle <sub>A</sub> ( $^\circ$ )	Angle <sub>B</sub> ( $^\circ$ )	
Case 1	10	1	0.1	1.5	20	10	
Case2	10	1	0.1	1.5	20	10	
Case3	10	1	0.1	1.5	20	10	

the frame at each point. Any point  $P_i$  is selected as the current grinding point of the cutting edge.

Step 2: Select any point on the arc chamfer of wheel, we define this point as the grinding point  $G$ .  $G$  can be represented in the coordinate system of wheel by equation  $[x_G \ y_G \ z_G]^T$  (Fig. 7). The angle  $\mu$  is the angle between the normal vector of the  $G$  and the axis of wheel, is a constant. The initial position of wheel is shown in Fig. 7. This position must satisfy the following requirements:

- a) The grinding point  $G$  must coincide with  $P_i$  that the origin of the frame.
- b) The normal vector of  $G$  and the binormal vector  $N_i$  are collinear.
- c) The axis of wheel must be in the plane that the plane contains  $N_i$ ,  $P_i$ , and  $T_i$ .

The rotational matrix  $R_5$  and the translational matrix  $M_5$  describe translation and rotation from  $O_w-X_w Y_w Z_w$  to  $P_i-T_i B_i N_i$  and are represented by

$$M_5 = \begin{bmatrix} 1 & 0 & 0 & x_G \\ 0 & 1 & 0 & y_G \\ 0 & 0 & 1 & z_G \\ 0 & 0 & 0 & 1 \end{bmatrix} \text{ and } R_5 = \begin{bmatrix} 0 & -\sin \mu & -\cos \mu & 0 \\ -1 & 0 & 0 & 0 \\ 0 & \cos \mu & -\sin \mu & 0 \\ 0 & 0 & 0 & 1 \end{bmatrix} \quad (18)$$

Step 3: To get the relief angle on the clearance, we rotate the wheel and the frame together around  $T_i$  by  $\alpha$ .  $\alpha$  can be continuously varied during the grinding process.  $\alpha$  is equal to relief angle (for details, see Chapter 4). We obtain a new frame  $P_{i1}-T_{i1} B_{i1} N_{i1}$ . Like Step 2, we can get the rotational matrix  $R_6$ , which is given by

$$R_6 = \begin{bmatrix} 1 & 0 & 0 & 0 \\ 0 & \cos \alpha & \sin \alpha & 0 \\ 0 & -\sin \alpha & \cos \alpha & 0 \\ 0 & 0 & 0 & 1 \end{bmatrix} \quad (19)$$

Step 4: Normally, the posture of the wheel can be controlled. The frame  $P_{i1}-T_{i1} B_{i1} N_{i1}$  and wheel are rotating around  $N_{i1}$ , and the rotational angle is  $\lambda_2$ .  $\lambda_2$  is set by users. We obtain a new frame  $P_{i2}-T_{i2} B_{i2} N_{i2}$ . Similarly, the rotational matrix  $R_7$  is represented

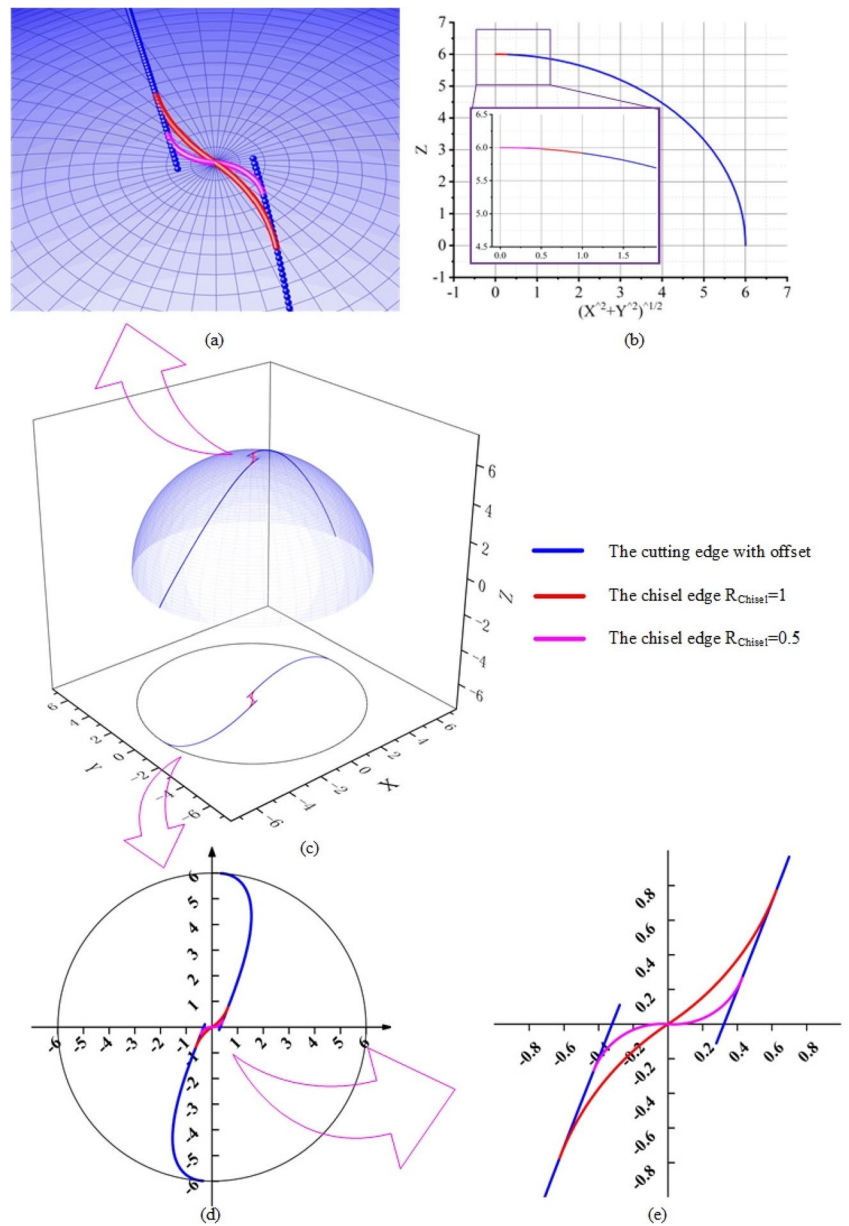
**Table 2** The parameters of the wheel

Grinding process	Type	Diameter (mm)	R1 (mm)	R2 (mm)	L <sub>w</sub> (mm)	$\varphi_w$ ( $^\circ$ )
Rake face	1A1	146.64	0.1	0.1	6	-15
Relief	11V9	96.995	0.1	0.1	20	45

**Table 3** The rotation angle

		No.1	No.2	No.3	No.4	No.5	No.6	No.7	No.8	No.9
Rake face	$\gamma$	-8	-6	-4	-2	0	2	4	6	8
Tip clearance	$\alpha$	0	2	4	6	8	10	12	14	16

**Fig. 9** The cutting edge and chisel-edge of the ball end mill



$$R_7 = \begin{bmatrix} \cos \lambda & -\sin \lambda & 0 & 0 \\ \sin \lambda & \cos \lambda & 0 & 0 \\ 0 & 0 & 1 & 0 \\ 0 & 0 & 0 & 1 \end{bmatrix} \quad (20)$$

The center position of the wheel can be expressed in the global coordinate system **O-XYZ** as

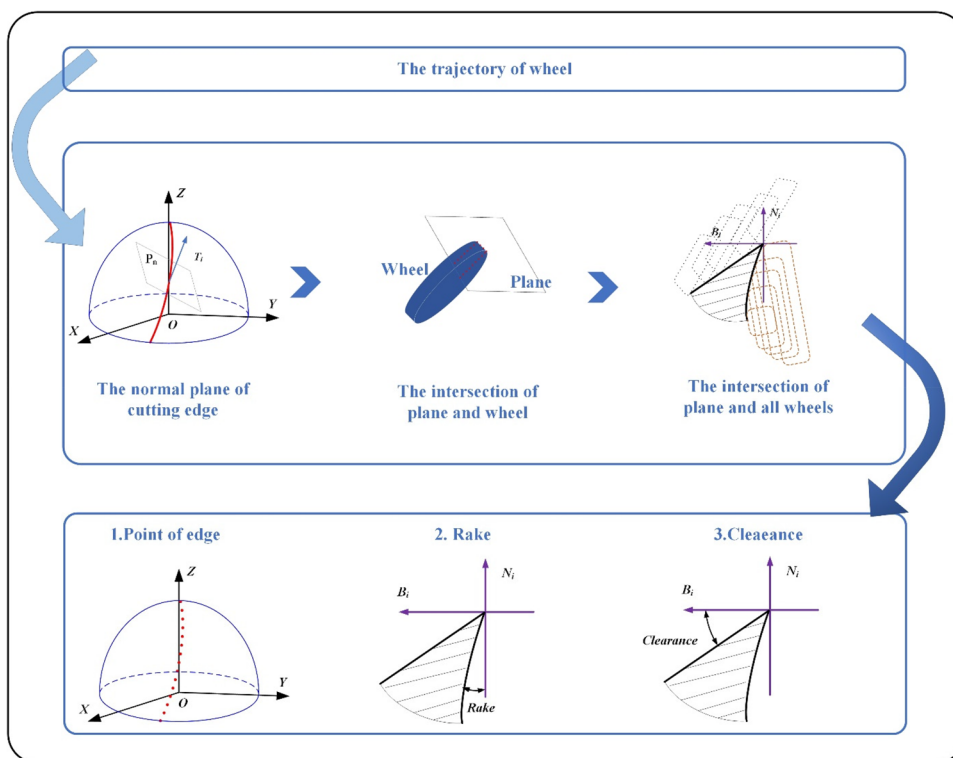
$$\begin{bmatrix} X_{Center} \\ Y_{Center} \\ Z_{Center} \\ 0 \end{bmatrix} = M_1 \cdot R_1 \cdot R_6 \cdot R_7 \cdot R_5 \cdot \left( M_5 \cdot \begin{bmatrix} x_w \\ y_w \\ z_w \\ 1 \end{bmatrix} \right) \quad (21)$$

The axis of the wheel can be expressed in the global coordinate system **O-XYZ** as

$$\begin{bmatrix} X_{Axis} \\ Y_{Axis} \\ Z_{Axis} \\ 0 \end{bmatrix} = M_1 \cdot R_1 \cdot R_6 \cdot R_7 \cdot R_5 \cdot \left( M_5 \cdot \begin{bmatrix} 0 \\ 1 \\ 0 \\ 0 \end{bmatrix} \right) \quad (22)$$

Figure 8 shows the process of calculating the trajectory of the clearance for the ball end mill.

**Fig. 10** Calculate rake angle and relief



## 4 Numerical example and experiment

In this section, the graphical method and experiments are used to demonstrate the algorithm. The effect of rotation angle on the rake angle and relief angle is also analyzed.

### 4.1 The parameters of ball end mill

Take a ball end mill with a radius of  $R = 12$  mm as an example to verify this model. The parameters of the ball end mill and the wheel are shown in Table 1 and 2.  $\gamma$  and  $\alpha$  are shown in Table 3. Cases 1 and 2 have chisel-edge; case 3 does not have a chisel-edge.

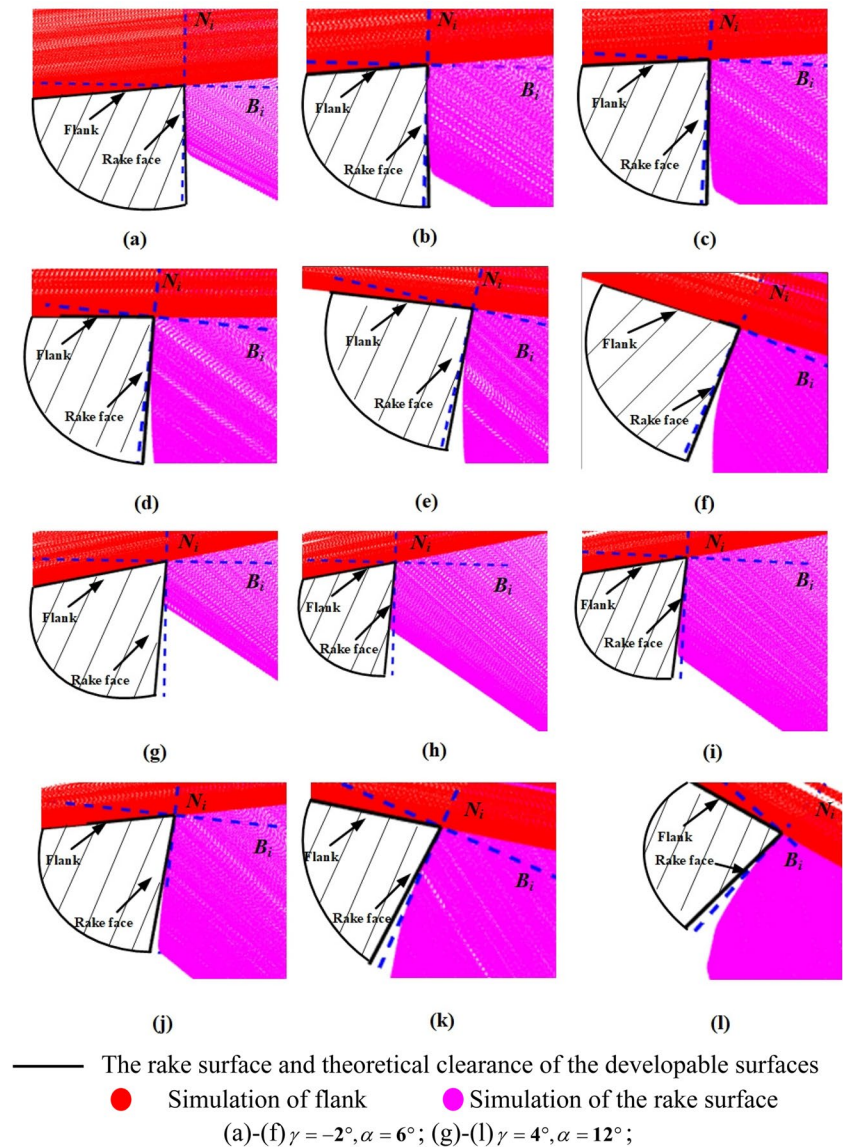
According to Section 2, we obtain the cutting edge, the chisel-edge, as shown in Fig. 9. From Fig. 9c, it can be seen that the cutting edge and the chisel-edge are on the spherical surface. As shown in Fig. 9a, the offset cutting edge doesn't pass the vertex of the spherical surface. However, the chisel-edges intersect the vertex of the spherical surface. The maximum value of the offset cutting edge is less than the radius in the  $z$ -axis direction, so it does not pass the vertex of the spherical surface. In the  $z$ -axis direction, the maximum value of the chisel-edge is equal to the radius, when  $z = R$ ,  $x = 0$ , and  $y = 0$ . So it passes the vertex of the spherical surface. Thus, the model of ball end mill with a chisel-edge has a better profile tolerance.

### 4.2 The simulation of the ball end mill

According to Sections 2 and 3, we can easily get the grinding path of the grinding wheel. The following is to get the normal rake angle, normal relief angle, and the cutting edge (Fig. 10): first, one point on the cutting edge is selected and its normal plane is determined. Next, the intersections of the normal plane and the surface of wheels on the grinding trajectory are calculated. The boundary of the intersections is the rake surface or flank (Fig. 11). Finally, we can easily calculate the cutting edge, rake angle, and relief angle.

As shown in Fig. 11, the intersection of the simulation rake face and the simulation clearance almost coincides with the theoretical cutting edge in all normal plans. This means that this model can accurately grind the designed cutting edge. The rake face of simulation is tangent to the rake face of the developable surfaces. This shows that the simulation the rake angle of the rake face to be equal to the rotation angle  $\gamma$ . For the relief angle, we can get the same conclusion. During the rotation angle  $\gamma$  from  $-8$  to  $8^\circ$ , the rake angle is still equal to the rotation angle (Fig. 12). The rotation angle  $\alpha$  from  $0$  to  $16^\circ$ , the relief angle is still equal to the rotation angle (Fig. 12). Therefore, the rotation angle  $\gamma$  is equal to the rake angle, and the rotation angle  $\alpha$  is equal to the relief angle.

**Fig. 11** The normal plane of cutting edge for the ball end mill



### 4.3 Experiment example

In this paper, the algorithm is demonstrated using experiments again. Case 1 and case 2 were implemented with chisel-edge in this paper. The chisel-edge radius of case 1 is 1 mm, and the chisel-edge radius of case 2 is 0.5 mm. Case 3 does not have a chisel-edge. In the experiment, the five axes grinding machine is BPX6 (Maker: BEIPING Machine). It contains three linear axes of motion XYZ and two axes of rotation BC, as shown in Fig. 13. The ball end mill was manufactured in Fig. 14. At the same time, the machining process of the machine was simulated using Solidpro, and the results are shown in Fig. 14. The chisel-edges of cases 1

and 2 are shown as yellow dashed lines. The chisel-edge of case 3 is formed by the intersection of the wheels. Its shape is not controlled and is related to the wheel and grinding parameters.

The profile tolerances of the ball end mill were measured and compared by Zoller Genius3, and the results are shown in Fig. 14. The profile tolerances of the ball end are within  $\pm 0.01$  mm. The profile tolerances of the ball end with chisel-edge at the vertex of the spherical surface are better than other mills. The errors in cases 1 and 2 are caused by measurement errors and machine motion errors. So, the chisel-edge part improves the model to have a better profile tolerance.



**Fig. 12** The normal plane of cutting edge for the ball end mill

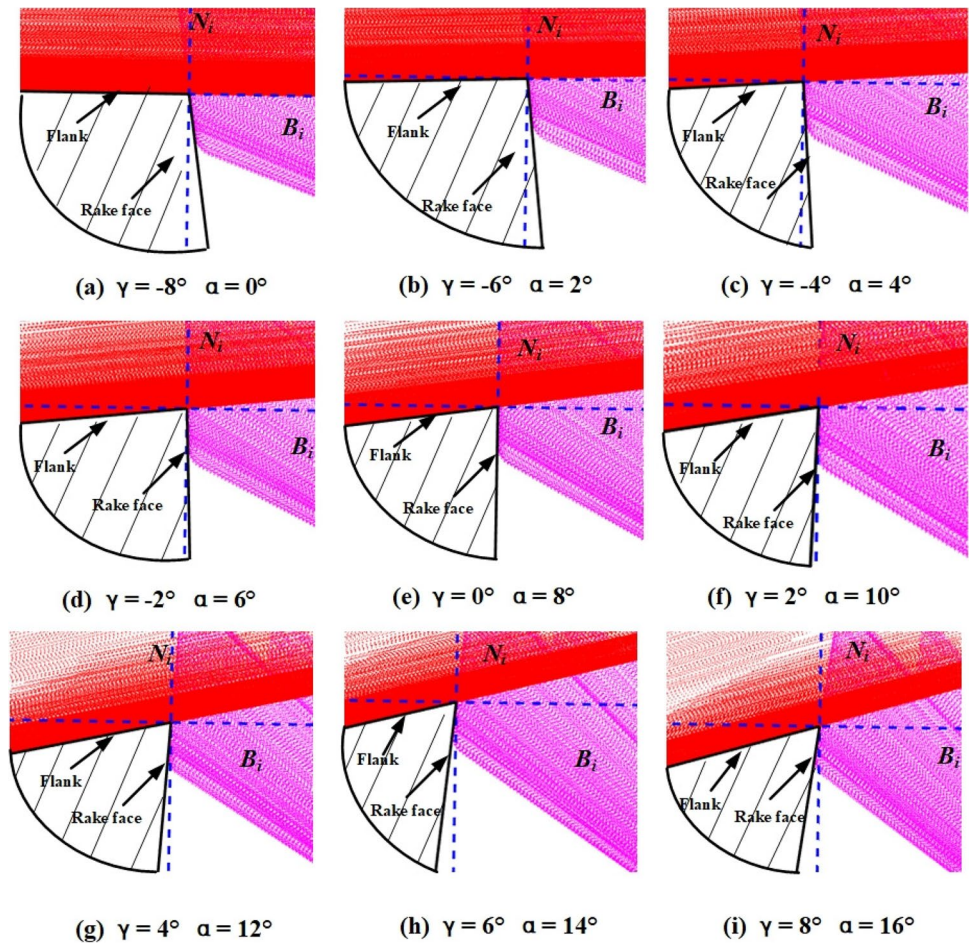


**Fig. 13** The five axes grinding machine

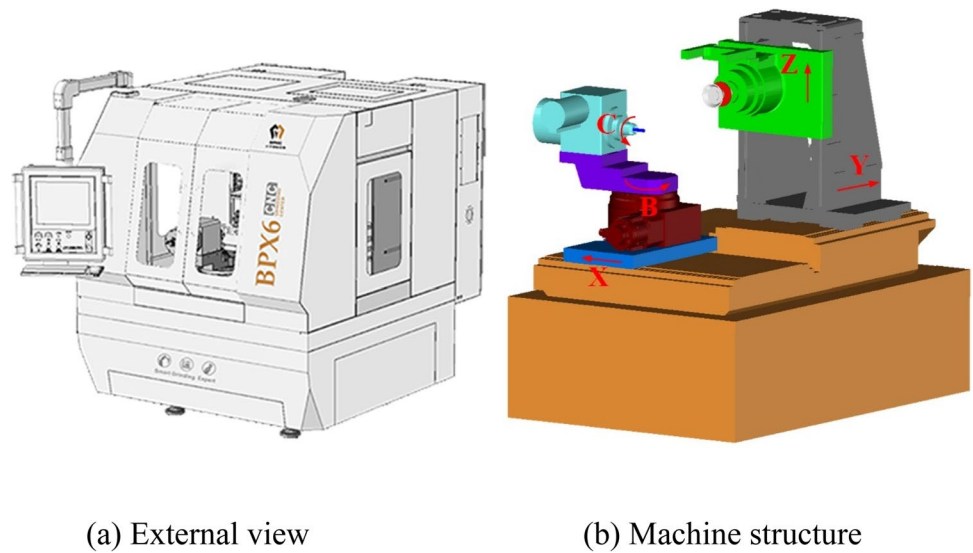
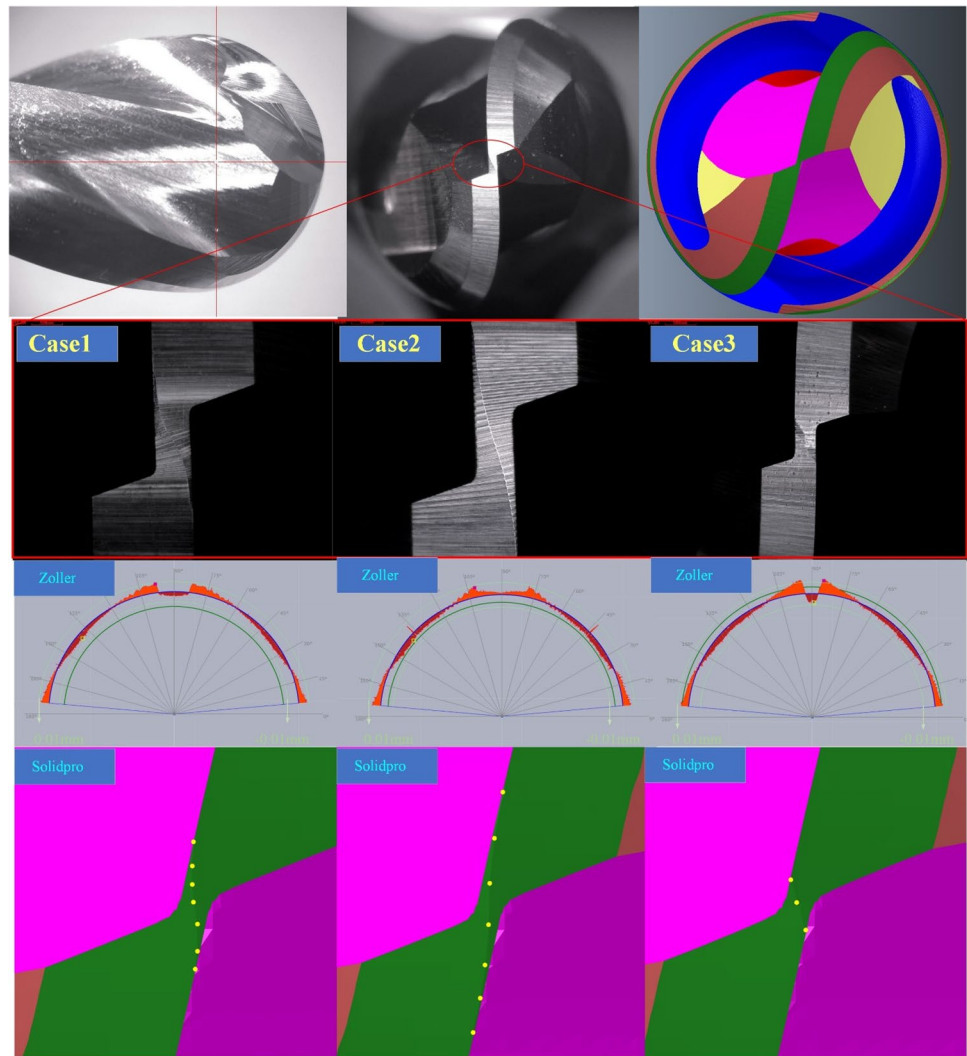


**Fig. 14** The manufacture, measurement, and simulation of the ball end mill



## 5 Conclusion

In this work, a new mathematical model of the ball end mill with a chisel-edge is presented. Then, the calculation method of grinding path for the rake surface and clearance is proposed. The model and grinding method of the ball end mill were verified by simulation and grinding experiments. This paper is summarized as follows:

1. The cutting edge was optimized, and the chisel-edge was also introduced into the model, which reduced the profile tolerance.
2. The calculation method of grinding path for the rake face by 1A1 wheel with arc chamfer is proposed. The calculation method of grinding path for the clearance by 11V9 wheel with arc chamfer is determined.
3. This model was proved by simulation. The simulation results show that the rotation angle  $\gamma$  and the normal rake angle are equal. The rotation angle  $\alpha$  is equal to the normal relief angle.
4. The model was further verified by grinding experiments. Compared to the ball end mill without a chisel-edge, the ball end mill made by this model has a higher profile tolerance.

This model improves the profile tolerances of the ball. But it has high requirements for the profile tolerances of wheel, especially for the grinding of chisel-edge. Our future work aligns with these directions, including cutting testing and compare cutting performance with other tools manufactured by other software.

**Supplementary Information** The online version contains supplementary material available at <https://doi.org/10.1007/s00170-023-12916-7>.

**Author contribution** Hongyang Wang: methodology, conceptualization, validation, writing—original draft, term, data curation. Xianli Liu: funding acquisition, writing—review and editing. Caixu Yue: writing—review and editing. Zhipeng Jiang: writing—review and editing, data curation. Gaojun Zheng: writing—review and editing, data curation. Kaiwang Zhao: writing—review and editing, data curation.

**Funding** This research was funded by projects of the International Cooperation and Exchanges NSFC (51720105009) and The National Key Research and Development Program of China (2019YFB1704800).

**Data availability** The datasets used or analyzed during the current study are available from the corresponding author on reasonable request.

**Code availability** Not applicable.

## Declarations

**Ethics approval** The content studied in this article belongs to the field of metal processing does not involve humans and animals. This article strictly follows the accepted principles of ethical and professional conduct.

**Consent to participate** My co-authors and I would like to opt in to In Review.

**Consent for publication** I agree with the Copyright Transfer Statement.

**Competing interests** The authors declare no competing interests.

## References

- Zhang W, Wang XF, He F, Xiong DL (2006) A practical method of modelling and simulation for drill fluting. *Int J Mach Tools Manuf* 46(6):667–672. <https://doi.org/10.1016/j.ijmachtools.2005.07.007>
- Ehmann KF, Devries MF (1990) Grinding wheel profile definition for the manufacture of drill flutes. *CIRP Ann Manuf Technol* 39(1):153–156. [https://doi.org/10.1016/s0007-8506\(07\)61024-5](https://doi.org/10.1016/s0007-8506(07)61024-5)
- Karpuschewski B, Jandecka K, Mourek D (2011) Automatic search for wheel position in flute grinding of cutting tools. *CIRP Ann Manuf Technol* 60(1):347–350. <https://doi.org/10.1016/j.cirp.2011.03.113>
- Nguyen VH, Ko SL (2013) Determination of workpiece profile and influence of singular point in helical grooving. *CIRP Ann Manuf Technol* 62(1):323–326. <https://doi.org/10.1016/j.cirp.2013.03.009>
- Nguyen H, Ko S-L (2014) A mathematical model for simulating and manufacturing ball end mill. *Comput Aided Des*. <https://doi.org/10.1016/j.cad.2014.01.002>
- Chen F (2009) Research on CNC grinding complex shaped cutter using spherical grinding wheel. *Huazhong University of Science and Technology*. <https://doi.org/10.7666/d.d088423>
- Lin SW, Lai HY (2001) A mathematical model for manufacturing ball-end cutters using a two-axis NC machine. *Int J Adv Manuf Technol* 17(12):881–888. <https://doi.org/10.1007/s001700170099>
- Cheng X, Ding G, Li R, Ma X, Qin S, Song X (2014) A new design and grinding algorithm for ball-end milling cutter with tooth offset center. *Proc Inst Mech Eng Part B J Eng Manuf* 228(7):687–697. <https://doi.org/10.1177/0954405413503318>
- Chen CB, Wang FS, Chang PC, Hwang JH, Chen WF (2006) A precision design and NC manufacturing model for concave-arc ball-end cutters. *Int J Adv Manuf Technol* 31(3–4):283–296
- Feng X (2002) Research on integrated virtual/solid CNC grinding of complex shape cutting tools. *Huazhong Univ Sci Technol*. <https://doi.org/10.7666/d.y451155>
- Ji W, Liu X, Wang L, Meng Y, Xuefeng W (2015) A study on geometry modelling of a ball-end mill with chamfered cutting edge. *J Manuf Proc* 19:205–211. <https://doi.org/10.1016/j.jmapro.2014.10.003>
- Yi Lu, Takeuchi Y, Takahashi I, Anzai M (2005) An integrated system development for ball end mill design, creation and evaluation. *Int J Adv Manuf Technol* 25(7–8):628–646. <https://doi.org/10.1007/s00170-004-2259-4>

**Publisher's Note** Springer Nature remains neutral with regard to jurisdictional claims in published maps and institutional affiliations.

Springer Nature or its licensor (e.g. a society or other partner) holds exclusive rights to this article under a publishing agreement with the author(s) or other rightsholder(s); author self-archiving of the accepted manuscript version of this article is solely governed by the terms of such publishing agreement and applicable law.